Volume 15
Number 12
21 June 2025
Pages 3455–3774

Catalysis Science & Technology

rsc.li/catalysis

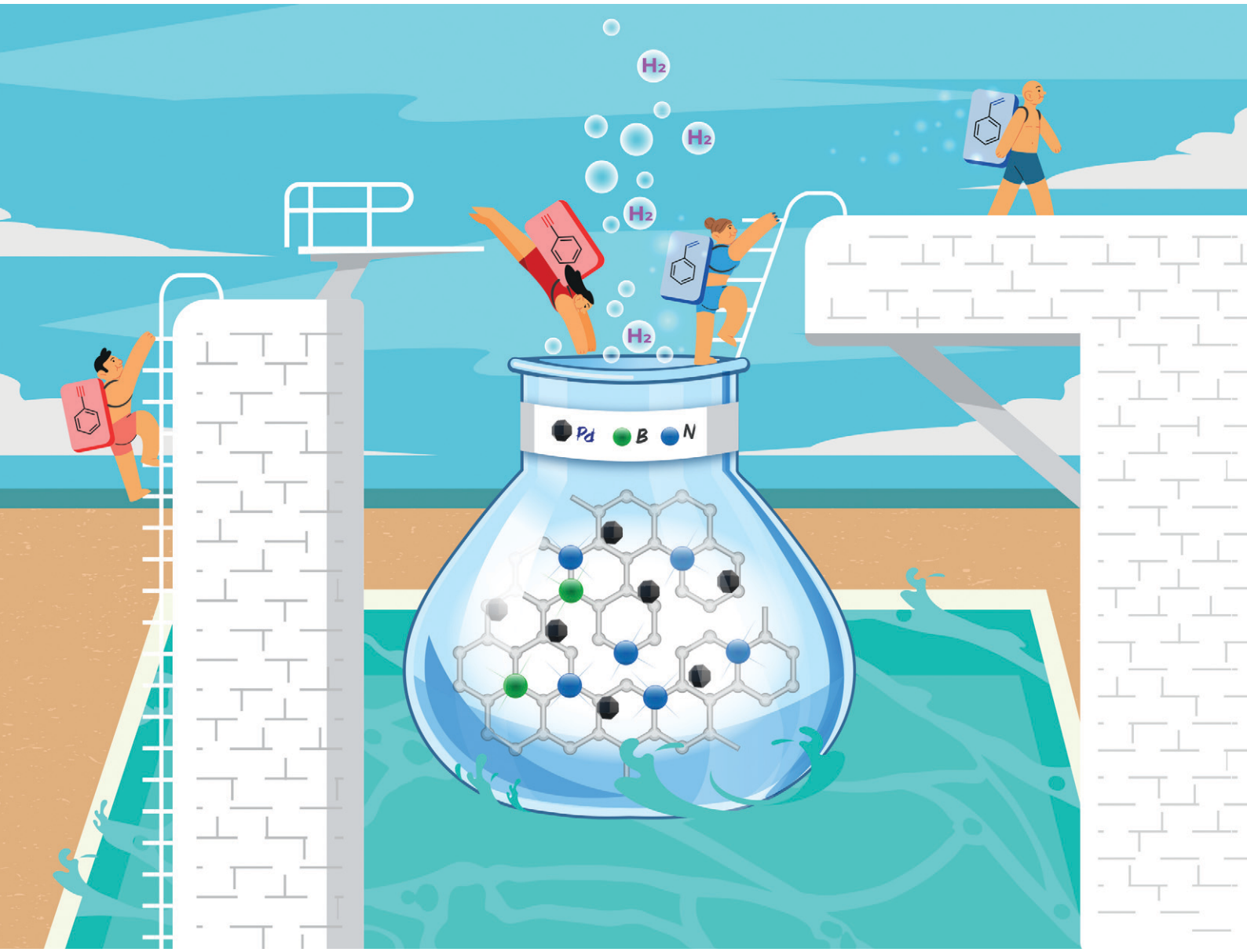

ISSN 2044-4761

ROYAL SOCIETY OF CHEMISTRY

PAPER
Adam W. Augustyniak
Double-doped **Pd/C_{N-B}** nano-architectures for hydrogen evolution and hydrogenation reaction in water

Catalysis Science & Technology

ROYAL SOCIETY OF CHEMISTRY

PAPER

View Article Online
View Journal | View Issue

Cite this: *Catal. Sci. Technol.*, 2025, **15**, 3536

Double-doped Pd/C_{N-B} nano-architectures for hydrogen evolution and hydrogenation reaction in water†

Adam W. Augustyniak

Carbon materials have shown great potential as catalyst supports. Rationally designing optimal precursors containing carbon, other heteroatoms, and metal precursors is crucial for the receipt of sophisticated materials for catalysis. In this regard, structurally and chemically defined metal–organic frameworks (MOFs) simultaneously contain key components of novel future catalysts and can be expected to be one of the most promising and versatile platforms for fabricating derived carbonaceous materials. Therefore, in this work, the thermal transformation of a unique Pd-MOF material is first proposed. The strategy also involved introducing tetrahydroxydiboron (THDB) as a B source for $[Pd(2\text{-pymo})_2]_n$ by physical grinding. During the carbonization process at 700 °C, the dual N–B doped carbon composite with small Pd nanoparticles (~4 nm) was formed. The hydrogen evolution reaction and the hydrogenation of phenylacetylene were selected to explore the catalytic performance of **Pd/C_{N-B}**. The TOFs of 56.6 mol H_2 mol cat^{-1} min^{-1} in NH_3BH_3 hydrolysis and 14.3 mol H_2 mol cat^{-1} min^{-1} in $B_2(OH)_4$ hydrolysis were reached. In the semihydrogenation of phenylacetylene, the **Pd/C_{N-B}** catalyst performs the highest conversion, 94%, with 97% selectivity of styrene at 70 °C. The synthetic approach demonstrated here can be extended in the future to prepare different carbon materials with other heteroatoms to improve catalytic performance.

Received 20th September 2024,
Accepted 29th April 2025

DOI: 10.1039/d4cy01128g

rsc.li/catalysis

Introduction

Metal–organic frameworks (MOFs) have received great attention and have been an unqualified success in many scientific fields due to their unique porous nature and exceptional diversity, structural properties, and chemical functionalities.[1–3] Many reports have confirmed the use of MOFs as catalysts for various reactions.[4–8] However, some MOFs suffer from low thermal stability. In addition, the use of an aqueous solution can cause an irreversible structure collapse. These issues limit their utility in catalysis and other applications. However, the relative instability of these materials can be used as another important feature.

MOFs are considered an ideal template/precursor for fabricating more stable metal/carbon-based nanostructures.[9] MOF-derived carbon materials can retain MOF-ordered structure and part of the porous nature but are also characterized by a uniform distribution of metals. The possibilities of heteroatom doping (*e.g.* N, S, P, B) make them excellent supports/hosts for metal nanoparticles. They can also be used to effectively tune their intrinsic properties, including electronic, surface and local chemical properties, as well as their mechanical properties.[10] The literature examples clearly show the existence of examples of N-doped carbon from MOFs as a catalyst for catalytic hydrogenation.[11–13]

For example, Chen and colleagues reported a Pd@CN catalyst consisting of Pd nanoparticles supported on N-doped carbon derived from ZIF-67 for phenol hydrogenation.[14] Likewise, Li *et al.* reported the Pd/carbon catalysts from the thermal transformation of ZIF-67 for selective semi-hydrogenation of phenylacetylene at mild conditions.[15] We recently presented the first synthesis of new carbon composites from $[Pd(2\text{-pymo})_2]_n$, a unique palladium MOF.[16] Carbonization of this Pd-MOF carried out in a N_2 atmosphere resulted in the formation of Pd/C_{PYMO} containing Pd NPs supported on N-doped porous carbon. These materials were used as catalysts for the transfer hydrogenation of phenylacetylene to styrene by $NaBH_4$.[16]

In recent years, intensive efforts have been achieved to exploit the potential of ammonia borane (NH_3BH_3) for hydrogen evolution catalysed by both noble and non-noble metals.[17–25] Furthermore, hydrolysis of tetrahydroxydiboron, $B_2(OH)_4$, is also promising for H_2 evolution. The most recent and intensive progress in this area is due to Astruc and collaborators.[26]

Palladium-based materials are unbeatable as catalysts in a large number of organic transformations, particularly in

Faculty of Chemistry, University of Wrocław, 14 F. Joliot-Curie St., 50-383 Wrocław, Poland. E-mail: adam.augustyniak@uwr.edu.pl

† Electronic supplementary information (ESI) available: TEM images, Raman, XRD, XPS, ^{1}H NMR, FT-IR, GC-FID, GC-MS. See DOI: https://doi.org/10.1039/d4cy01128g

hydrogenation processes.[27] Carbon-based catalysts are a mainstay of the catalyst industry, and their significance is underscored by the prevalence of Pd/C as an economical and easily recyclable catalyst. Moreover, it is notable that more than 75% of hydrogenation reactions occur in the presence of Pd/C catalyst.[28] However, there are indications that the price of Pd will continue to rise as this material is rapidly consumed. Consequently, there is an urgent need to focus on the design of new, advanced catalysts that can reduce the amount of Pd used while simultaneously increasing their activity and stability. The size, shape and electronic properties of Pd nanoparticles have a significant impact on their catalytic properties and stabilities. The use of a $[Pd(2\text{-pymo})_2]_n$ MOF as a matrix for the preparation of carbon materials allows these parameters to be controlled. The nitrogen-rich organic ligands from $[Pd(2\text{-pymo})_2]_n$ MOF form functional groups over the surface of carbons, which can minimize their Pd agglomeration and regulate the electronic properties of the metal.

A further advantage of using $[Pd(2\text{-pymo})_2]_n$ MOFs is that they can be easily modified by introducing additional heteroatoms. The present research on hydrogenation catalysts focuses on boron-containing materials. In this context, Zhao *et. al.* have recently reported highly promising results concerning the dehydrogenation of formic acid catalysed by Pd/C of boron-doped.[29] Similarly, Zhang *et. al* have demonstrated the potential to regulate the selectivity of acetylene catalytic hydrogenation by Pd catalysts doped with B/C atoms in the subsurface.[30]

In view of the above, the preparation of B-containing or dual N–B carbons from MOFs remains a challenge and their potential has not yet been exploited, especially in catalytic hydrogen generation and hydrogenation reactions. Therefore, the strategy proposed here was to introduce tetrahydroxydiboron (THDB) as a B source to $[Pd(2\text{-pymo})_2]_n$ by physical grinding. The synergistic effect between the heteroatoms and palladium renders the resulting new material a catalyst for hydrogen evolution from NH_3BH_3, $B_2(OH)_4$, and phenylacetylene hydrogenation. This work reveals a novel strategy to achieve heteroatom-doped carbon catalysts using Pd-MOF as a precursor for carbon matrices and may be useful to scientists developing efficient Pd/C catalysts for hydrogenation reactions.

Experimental

Materials and chemicals

All chemicals were used as received without any further purification. Potassium tetrachloropalladate(II) (K_2PdCl_4, 98%), 2-hydroxypyrimidine hydrochloride (Hpymo·HCl, 98%), phenylacetylene (99.8%), 4-ethynyltoluene (97%), 3-ethynylanisole (97%), 3-nitrophenylacetylene (97%), chloroform (99.8%), $CDCl_3$ (≥99.8 atom % D, contains 0.5 wt% silver foil as stabilizer), D_2O (99.9 atom % D), Pd/C 10 wt%, and RANEY®-nickel were purchased from Sigma-Aldrich. Ammonia borane (NH_3BH_3, 90%) and hypodiboric acid ($B_2(OH)_4$, 97%) were purchased from BLD Pharm Germany. For the temperature-programmed desorption (TPD) test, He (5 N Air Products), 0.5% NH_3 (Union Carbide) and 5% CO_2/He (Air Liquide) were used. Milli-Q water (18.2 MΩ) was used for all experiments.

Catalyst preparation

The $[Pd(2\text{-pymo})_2]_n$ and *trans*-$[PdCl_2(Hpymo)_2]$ were prepared with some modifications.[31] The *trans*-$[PdCl_2(Hpymo)_2]$ (3.675 g, 10 mmol) was added to an aqueous solution of NaOH (0.399 g, 4 mmol). The mixture was refluxed for one day. Finally, yellow microcrystalline powder of $[Pd(2\text{-pymo})_2]_n$ was obtained. The product was filtered and washed with water (2 × 20 mL) and acetone (2 × 5 mL) and dried under a vacuum. The Pd content was 23 wt% (ICP-OES).

$Pd/C_{B–N}$ preparation

Typically, 0.3 g of $[Pd(2\text{-pymo})_2]_n$ and 0.2 g of THDB were mixed and ground in a mortar for *ca.* 10 min. The mixture was then transferred to a ceramic crucible and heated in a tube furnace at 700 °C for 2 h in an N_2 flow. EA (%) C 17.28, N 5.39, H 0.78. The Pd content was 49.9 wt% (XRF) and the B content was 5.7 wt% (ICP-OES) (Table S1†).

Catalytic tests

Phenylacetylene transfer hydrogenation

The transfer hydrogenation reaction was performed in a glass vial (12 mL). The catalyst (0.5–1 mol%), phenylacetylene (0.91 mmol), NH_3BH_3 (1 mmol) or THDB (1 mmol), and water (2 mL) were introduced into a bottle, and then the bottle was sealed and placed in an aluminum block and heated to 50–70 °C for 10–40 min. At the end of the reaction, the catalyst was separated by centrifugation, and the organic products were extracted with $CHCl_3$ (5 mL) and analyzed by means of GC-FID, GC-MS and ^1H NMR.

H_2 evolution

$Pd/C_{N–B}$ (0.5 mol%) and 2 mL of water were placed in a two-necked flask and stirred. Then an aqueous suspension (2 mL) containing NH_3BH_3 (1 mmol, 30 mg) or THDB (1 mmol, 90 mg) was added to the flask, and the resulting mixture was stirred at 700 rpm and heated to 25–70 °C. Then, a graduated cylinder with water was connected to the reaction flask to measure the volume of evolved H_2.

Characterization

X-ray diffraction (XRD) patterns were recorded with a powder X-ray diffractometer D8-ADVANCE Bruker (Cu Kα, λ = 1.54056 Å). X-ray fluorescence (XRF) was performed using Panalytical Axios mAX, Rh SS-mAX, 4 Kw. Transmission electron microscopy (TEM) images were performed using a FEI Tecnai G2 20 X-TWIN and Titan G2 60–300 kV microscope. Scanning transmission electron microscopy (STEM) images were

performed using a SCIOS 2 microscope Thermo Fisher Scientific. X-ray photoelectron spectra (XPS) were recorded using a UHV Prevac X-ray photoelectron spectrometer, VG Scienta SAX 100 equipped with Al Kα radiation (1486.6 eV). Inductively coupled plasma analysis (ICP-OES) was carried out in an iCAP 7400 DUO icp (Thermo Fisher Scientific). A Vario EL Cube CHNS elemental analyzer was used for elemental (C, H, N) analyses. IR spectra were recorded on a Bruker 66/s FT-IR spectrometer. ^{1}H-NMR spectra were recorded on a Bruker 500 MHz spectrometer using $CDCl_3$ (7.26 ppm). ^{13}C and ^{11}B MAS solid-state NMR experiments were performed with spectrometer Jeol JNM-ECZ500R 500 MHz with 3.2 mm AutoMAS DR. MicroRaman apparatus (inVia™ Renishaw) was used to register Raman spectra (514 nm). GC-MS analyses were carried out using a Shimadzu QP201OSE gas chromatograph. TPD measurements were carried out using AMI-1 (Altamira Inst.) combined with a mass spectrometer HPR20 (Hiden Analytical).

Results and discussion

Catalyst characterisation

A new catalyst **Pd/C$_{N-B}$** was prepared by co-carbonization of the mixture $[Pd(2\text{-pymo})_2]_n$ MOF and THDB in a nitrogen flow at 700 °C (Fig. 1a). TEM was used to characterize the morphology and size of Pd nanoparticles in the **Pd/C$_{N-B}$** catalyst. As demonstrated, part of Pd nanoparticles exhibit a spherical morphology and deposit well on the carbon matrice (Fig. 1b). The corresponding Pd NP size distributions (Fig. S1c†) showed that Pd NPs are average sizes of 4 nm, which are consistent with the calculated by the Scherrer equation based on the XRD patterns (5.3 nm). The high-resolution TEM images were used to investigate the lattice spacing of the Pd NPs and to confirm their crystallinities (Fig. 1b, S1a and b†). The lattice spacing of 2.29 Å corresponds to the (111) plane of zero-valent Pd.[32] The appropriate elemental mappings in Fig. 1c–g showed uniform C, B, N and Pd distributions.

The chemical structure of the **Pd/C$_{N-B}$** catalyst was first investigated by XRD, Raman, FT-IR, and ^{13}C and ^{11}B solid-state NMR spectroscopy. XRD pattern (Fig. 2a) showed that the characteristic diffraction peaks of metallic Pd are clearly observed at 2θ = 40.1° (111), 46.8° (200), 68.3° (220), and 82.3° (311), which is in good agreement with the previous works.[33]

The Raman spectra showed two characteristic peaks centered at 1356 and 1602 cm^{-1} (Fig. 2b), corresponding to the D and G bands of carbon.[34] The intensity ratio of the D and G bands (I_D/I_G) was 1.06, which is higher than that of the undoped boron catalyst **Pd/C$_{PYMO}$** (I_D/I_G = 0.91) (Fig. S2†), suggesting the existence of more defects for the **Pd/C$_{N-B}$** sample. The surface structure of **Pd/C$_{N-B}$** analyzed by FT-IR (Fig. S3†) revealed the wide absorption bands located at 3419 and 3204 cm^{-1}, which may be caused by the stretching vibration of N–H and O–H, respectively.[35] The band at 1576 cm^{-1} represents the stretching vibration of C=C. The broad absorption band located around 1480–1000 cm^{-1} confirms the existence of B–N, B–C, and B–OH vibration.[36] The band at 782 cm^{-1} represents the vibration of B–N–B.[36] Further, the single broad signal between 100 and 160 ppm (Fig. 2c) in ^{13}C NMR MAS spectrum can be attributed to aromatic carbons in **Pd/C$_{N-B}$** architectures. The signal around −14 ppm in ^{11}B NMR MAS spectra can be assigned to B–N, B–C bonds (Fig. 2d). The chemical shift ranges correspond to tetracoordinate boron atoms.[37] In order to characterize the acid/basic properties of the **Pd/C$_{N-B}$** catalyst the CO_2-TPD and NH_3-TPD was performed and the profiles of obtained curves are plotted in Fig. S4a.† TPD-NH_3 curves obtained after heating the sample in He to 400 °C. Ammonia adsorption was carried out after cooling the sample to 100 °C. The shape of the NH_3-TPD curves indicates the presence of acidic adsorption centres with a similar NH_3 binding strength.

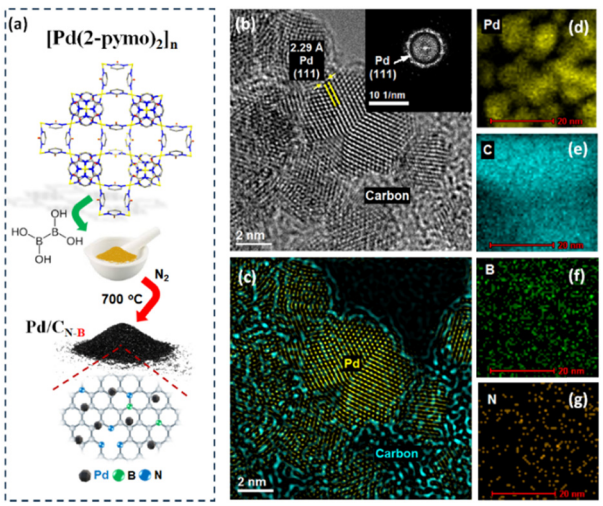

Fig. 1 Diagram of the synthesis (a), HR-TEM with inset the FFT (b), element mappings (d–g), and RGB image (c) of **Pd/C$_{N-B}$** catalyst.

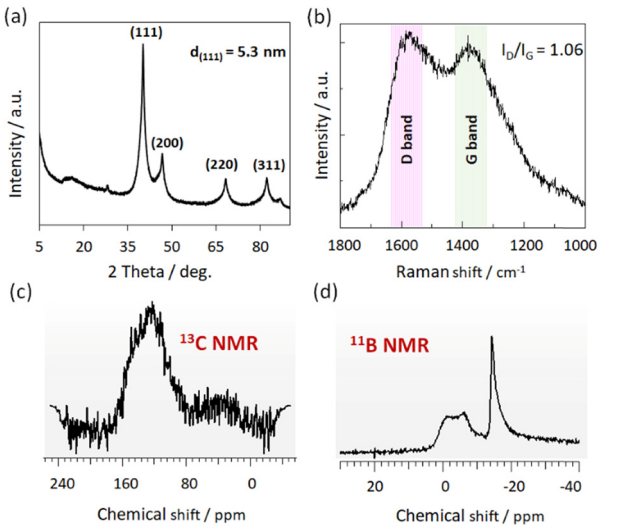

Fig. 2 XRD pattern (a), Raman spectrum (b), solid-state ^{13}C NMR (c) and solid-state ^{11}B NMR (d) of **Pd/C$_{N-B}$** catalyst.

Despite heating the sample at 400 °C for 30 min, the curve shows an increase in the intensity of the signal indicating CO_2 release at an elevated temperature (approx. 350 °C). This effect is likely attributable to the subsequent decomposition of the relevant functional groups present within the carbon matrix. The TPD-CO_2 profile is shown in Fig. S4b.† The CO_2 adsorption step was carried out after the material had been heated to 400 °C and then cooled to 100 °C. The shape and size of the CO_2 desorption peak indicates the presence of relatively strong basic centres.

Catalytic activity evaluation

In our previous paper, we presented a composite **Pd/C$_{PYMO}$** that had been obtained from the thermal conversion of $[Pd(2\text{-pymo})_2]_n$. This composite catalyzed the hydrogenation of phenylacetylene using $NaBH_4$ as the hydrogen source, but some excess $NaBH_4$ was necessary.[16] The current investigation is exploring alternative hydrogen sources, including NH_3BH_3 and $B_2(OH)_4$, to achieve high yields and excellent selectivity for both alkyne semi-hydrogenation and hydrogen production over the **Pd/C$_{N-B}$** catalyst. Fig. 3 displays the catalytic activity of **Pd/C$_{N-B}$** for the hydrolytic dehydrogenation of NH_3BH_3 and $B_2(OH)_4$.

It can be seen that **Pd/C$_{N-B}$** is catalytically active without observable induction periods for NH_3BH_3 hydrolysis, producing 3 mmol of H_2 per 1 mmol of NH_3BH_3. It can be clearly seen that the **Pd/C$_{N-B}$** exhibits a much higher catalytic activity as the reaction temperature is increased. The 9.3 min is needed for the complete hydrolysis of NH_3BH_3 at 50 °C when 6 and 2.7 min at 60 and 70 °C resulting in TOF values (calculated by 10% substrate conversion) 15.5, 31, and 56.6 mol H_2/(mol Pd min)$^{-1}$, respectively (Fig. 3). As for the catalytic NH_3BH_3 hydrolysis, **Pd/C$_{N-B}$** is also active for the $B_2(OH)_4$ hydrolysis. In this case, 1 mmol of $B_2(OH)_4$ (90 mg) is consumed, and 1 mmol of H_2 is produced, corresponding to 22.4 mL. Interestingly, in the case of $B_2(OH)_4$, complete hydrolysis was observed at 87.7 s at 25 °C with a TOF value of 7.14 mol H_2/(mol Pd min)$^{-1}$. The $B_2(OH)_4$ hydrolysis reaction catalyzed by **Pd/C$_{N-B}$** was further performed at different temperatures (35 and 45 °C), leading to an increased reaction rate with corresponding TOF values of 13.6 and 14.3 mol H_2/(mol Pd min)$^{-1}$.

Hydrolysis of NH_3BH_3 and $B_2(OH)_4$ can be an easy hydrogen source for hydrogenation reactions. In order to evaluate the catalytic performance of the **Pd/C$_{N-B}$**, the semi-hydrogenation of phenylacetylene was selected as a model system.

The selectivity and conversion rates for a series of reactions conducted at varying times and temperatures have been examined. When NH_3BH_3 was used as the hydrogen source, phenylacetylene hydrogenation experiments were carried out at 50–70 °C (Fig. 4a). At 50 °C, after 10 min, 41% of phenylacetylene was converted to styrene, and conversion increased to 70% after 40 min. A significant increase in conversion was achieved at a higher temperature. At 70 °C, conversion increased to 80% in 10 min. More importantly, the selectivity to styrene was very high at over 95% (Fig. 4b). The temperature dependence of the hydrogenation rate was used to calculate the activation energy (E_a) (Fig. 4c). Based on the Arrhenius relation, $k = A\cdot\exp(-E_a/RT)$, the activation energy was determined to be 84.48 kJ mol^{-1} (Fig. 4c and S5†). This value of activation energy is slightly higher than for the commercially available catalyst Pd/C (51.5 kJ mol^{-1}). However, a high selectivity towards styrene is maintained.[38]

To evaluate the effect of 0.5 mol% amount of the **Pd/C$_{N-B}$** catalyst, we carried out additional experiments (Fig. S6†).

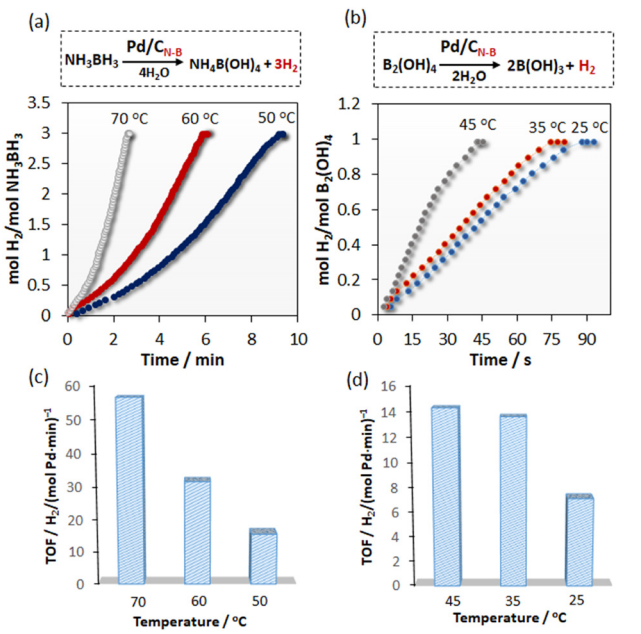

Fig. 3 Time plot of H_2 evolution from the hydrolysis of NH_3BH_3 (a) and $B_2(OH)_4$ (b), TOF values for 10% substrate conversion catalyzed by **Pd/C$_{N-B}$** (c and d).

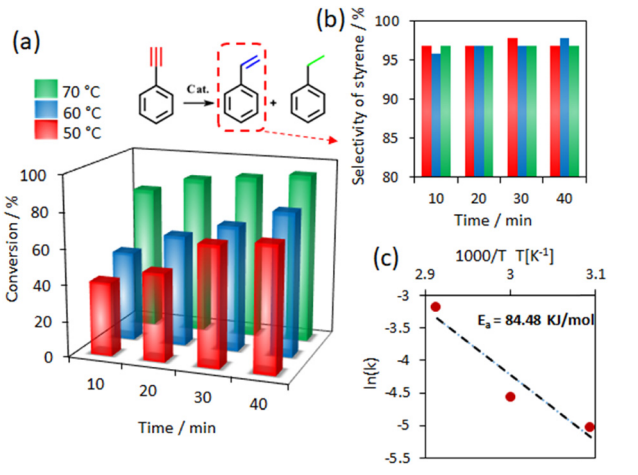

Fig. 4 The time profiles of conversion of phenylacetylene catalyzed by **Pd/C$_{N-B}$**. Reaction conditions: 0.91 mmol of phenylacetylene, catalyst (1 mol% Pd), Pd : NH_3BH_3 = 0.0091, 2 mL of H_2O (a). Effect of reaction time on the selectivity of styrene (b) and Arrhenius plot of ln(*k*) *versus* 1000/*T* (c).

For this case, only 60% of phenylacetylene was converted during 40 min at 70 °C, whereby the selectivity to styrene was still very high. Then, the hydrogenation of 1 : 1 mixture of styrene and phenylacetylene was also tested (Fig. S7†). At 50 °C, phenylacetylene was completely converted to styrene. Nevertheless, the high selectivity for styrene was maintained during the extended reaction time of 60 min, with only negligible ethylbenzene being detected. This result is significant because maintaining such selectivity over longer reaction times may be interesting for practical purposes.

Subsequently, $B_2(OH)_4$ was used to investigate the effect of the alternative H_2 source on the hydrogenation of phenylacetylene. The reactions were carried out at 45 °C. Interestingly, phenylacetylene conversions for 0.5 mol% of **Pd/C$_{N-B}$** were below 1% during 40 min. An increase in the amount of catalyst to 1 mol% results in a 70% conversion of phenylacetylene. Unfortunately, the selectivity in this case was not satisfactory, and it was only 87% for styrene (Fig. S8†). Accordingly, in the studied hydrogenation reaction system, NH_3BH_3 demonstrated the most favorable effect, consistent with the findings of the preceding report.[39]

In order to gain further insight into the catalytic activity of **Pd/C$_{N-B}$** for chemoselective hydrogenation, a more refined substituted phenylacetylenes such as 3-nitrophenyloacetylen, 3-ethynylanisole and 4-ethynyltoluene have been studied (Tables S2–S4†). The **Pd/C$_{N-B}$** catalyst exhibits excellent conversion (100%) but poor selectivity in the hydrogenation of 3-nitrophenylacetylene. At 60 °C, the catalyst facilitates the direct hydrogenation of 3-nitrophenylacetylene to 87.4% of 3-ethylaniline and 12.6% of 1-ethyl-3-nitrobenzene (Table S2 and Fig. S9†). The highest selectivity to 3-nitrostyrene was achieved at 40 and 50 °C, with a similar selectivity of 39.4 and 40.8%, respectively (Fig. S10†). On the other hand, complete conversion of 3-ethynylanisole was achieved; however, the process was accompanied by a low level of selectivity, with only 16% of the reaction proceeding towards alkene formation (Table S3 and Fig. S11 and S12†). Meanwhile, for 4-ethynyltoluene hydrogenation it was found that the desired alkene product can be obtained in good selectivity (95%), although the substrate conversion was only 79% (Table S4 and Fig. S13 and S14†).

Finally, the two commercial catalysts such as Pd/C (10 wt%) and RANEY®-nickel were used in the same reaction conditions. In the case of Pd/C, a 72% conversion of phenylacetylene and 95% selectivity to styrene was achieved (Fig. S15†) Concurrently, RANEY® nickel exhibited a high degree of styrene selectivity (100%) while demonstrating low phenylacetylene conversion (22%) (Fig. S16†). The previously published undoped boron **Pd/C$_{PYMO}$** catalyst was also tested under the same reaction conditions, but the conversion of phenylacetylene was negligible in this case (Fig. 17†).

Moreover, the reusability of **Pd/C$_{N-B}$** as a heterogeneous catalyst was investigated. **Pd/C$_{N-B}$** was reused over four successive cycles, without any visible loss of catalytic activity (Fig. S18†). The **Pd/C$_{N-B}$** catalyst was analyzed by different techniques before and after catalytic reactions. After

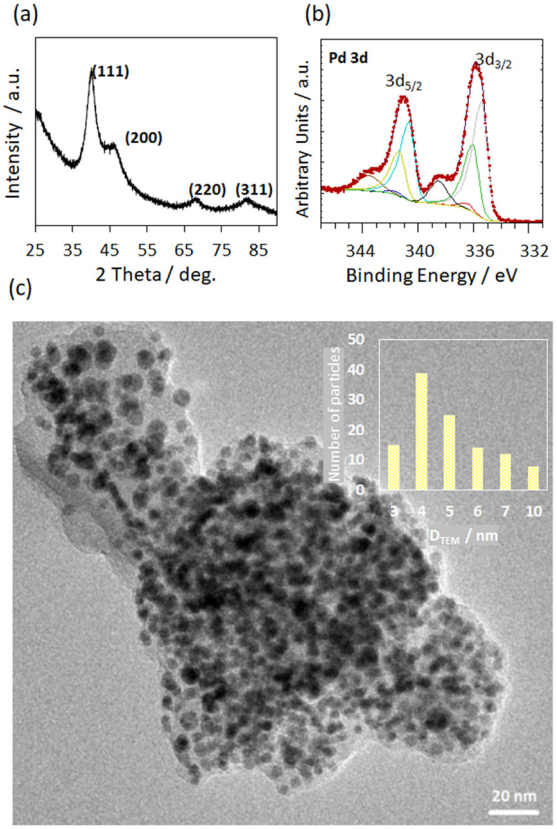

Fig. 5 XRD pattern (a) and XPS spectrum (b) of the Pd 3d region, and TEM image with inset the particle size distributions (c) of **Pd/C$_{N-B}$** after catalytic phenylacetylene hydrogenation.

phenylacetylene hydrogenation XRD analysis confirmed the existence of Pd nanoparticles with average size of 3.6 nm calculated by the Scherrer equation (Fig. 5a), which is in good agreement with the average size determined from TEM images (Fig. 5c). Interestingly, the size of the palladium nanoparticles has decreased compared to the original material. In the case of **Pd/C$_{N-B}$** after H_2 evolution catalyst remained almost unchanged (Fig. S19 and S20†). This is probably related to the possibility of partial dissolution of Pd nanoparticles during the catalytic reaction. The ICP-OES measurements taken for the post-reaction solutions showed small amount of palladium in the solution proving this hypothesis (Fig. S21†). It is worth noting that the palladium content in the post-reaction mixture is much higher when commercial Pd/C is used, which confirms the greater stability of the **Pd/C$_{N-B}$** system.

The surface conditions of the catalyst in use were further investigated by means of the XPS technique (Fig. 5b and S22†). For the 3d XPS core level region, four components are observed and can be attributed to the metallic Pd(0) and Pd(II) species. The binding energies at $3d_{5/2}$ = 335.5, 336.0, 336.4, and 338.4 eV can be ascribed to Pd(0), Pd(0)–B/C, PdO and other Pd(II) forms, respectively.[40,41] However, the relatively high concentration of Pd(0) species, about 87%, suggests that the Pd(II) species can be mainly the result of

oxidation of the outer metal surface. The main component C 1s at 284.9 eV can be assigned to (C–C/C–H) species, while the peaks at around 284.3, 286.5, and 287.0 eV are due to C–B/B–C–N2, C–N3, and C–O bonding, respectively.[42,43] The N 1s spectrum is composed of four components at 398.0 eV, signed for (N–B3) and 398.9, 400.2, and 402.6 eV, belonging to pyridinic-N, pyrrolic-N, and oxidized-N, respectively.[3,36] Correspondingly, the boron species existed in the form of B–N_3/B–C (190.4 eV), O–B–N_2/B–C_2–O (191.4 eV), B–C–O_2 (192.3 eV) and H_3BO_3 (193.1 eV).[44]

Mechanistic study

In order to gain further insight into the hydrogenation process and the differences between the activities of NH_3BH_3 and $B_2(OH)_4$, additional experiments were conducted. As previously reported, the pivotal role of water in the reaction was identified. Whatever use of NH_3BH_3 or $B_2(OH)_4$, the hydrogen species may come directly from water in each case. This is confirmed by the ^{1}H NMR spectra indicating D (deuterium) substitution in styrene (Fig. S23 and S24†). The rate of hydrogen generation is a critical factor that can influence the selectivity of the reaction. The use of NH_3BH_3 led to active hydrogen species $H^{\delta-}$ from B–H and H_2O cleavage, which react with alkynes instead of producing H_2. When $B_2(OH)_4$ is used, gaseous H_2 is constantly produced, which then undergoes homolytic cleavage to give two active hydrides. The next hydride formed after homolytic dissociation can move to the near-surface region of the metal counterparts, forming the subsurface hydride leads to the low selectivity of styrene (path A).[45] In path B, the styrene formed exhibits a weak interaction with the polar hydrogen species, thereby inhibiting over-hydrogenation (Fig. 6).

The next hydride formed after homolytic dissociation can move to the near-surface region of the metal counterparts, forming the subsurface hydride leads to the low selectivity of styrene (path A).[44] In path B, the styrene formed exhibits a weak interaction with the polar hydrogen species, thereby inhibiting over-hydrogenation. To support this hypothesis, an experiment was carried out using a tandem reactor (Fig. S25†). In one chamber, 1 mmol of $B_2(OH)_4$ and **Pd/C_{N-B}** (1 mol%) and 2 ml of H_2O were placed. In the second chamber, on the other hand, 1 mmol phenylacetylene in 2 ml H_2O and **Pd/C_{N-B}** were placed. The *in situ* H_2 generation resulted in non-selective hydrogenation of phenylacetylene, thereby confirming the aforementioned hypothesis. However, only 44% of the phenylacetylene was converted (Fig. S25†). Accordingly, in the case of $B_2(OH)_4$, two alternative reaction pathways of hydrogenation can be considered, as illustrated in Fig. 6.

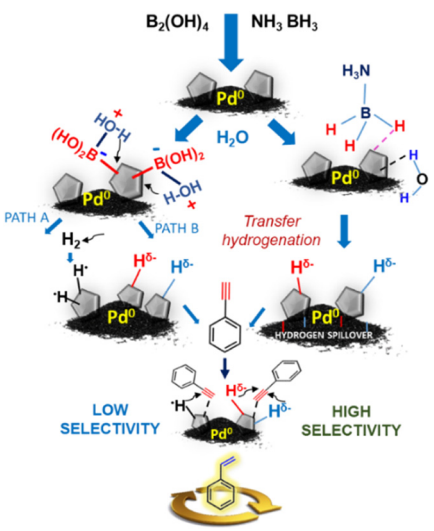

Fig. 6 Proposed mechanism of phenylacetylene hydrogenation.

The high selectivity to styrene can also be attributed to the presence of Lewis acid centres in the carbon matrix. In support of this hypothesis, the hydrogenation of phenylacetylene was conducted as a probe reaction to explore the possible influence of acid places in carbon matrice. The hydrogenation of phenylacetylene was performed by introducing ammonia water into the reaction system in order to deactivate the acid centres.

As demonstrated in Fig. S26,† the selectivity towards styrene was found to be entirely absent, with the predominant product being ethylbenzene. Earlier reports indicated that doping the carbon carrier with heteroatoms, including boron, can facilitate the migration of dissolved hydrogen to the surface of the carrier, ensuring much better activity and selectivity of hydrogenation.[46] This hypothesis was confirmed in this case.

Conclusions

To summarise, the preparation of active and stable heterogeneous Pd-based N–B doped carbon catalyst obtained by thermal conversion of Pd MOF is demonstrated. The introduction of a boron atom into the carbon matrix is an effective strategy to improve activity compared to the undoped system. The **Pd/C_{N-B}** catalyst was proved to be a highly active catalyst in the hydrogen evolution from boron compounds and phenylacetylene hydrogenation.

In the case of NH_3BH_3 and $B_2(OH)_4$, complete hydrolysis was observed at 9.3 min at 50 °C and 87.7 s at 25 °C, respectively.

It was found that the use of NH_3BH_3 leads to the transfer hydrogenation of phenylacetylene with high selectivity of styrene. In the case of $B_2(OH)_4$, a different trend was observed. Hydrogen gas was produced from the hydrolysis of $B_2(OH)_4$ and then, after homolytic dissociation, phenylethylene underwent hydrogenation. In this case, the selectivity to styrene was found to be lower. TPD results show that boron sites on carbon material probably play a critical role in H spillover. Deactivation of Lewis acid centres by adding ammonia water resulted in a complete loss of selectivity towards styrene.

The results presented in this work may serve as a source of inspiration for the development of new heteroatom-doped carbon catalysts for other challenging organic transformations.

Data availability

The data that support the findings of this study are available from the corresponding author, upon reasonable request.

Conflicts of interest

There are no conflicts to declare.

Acknowledgements

This research project is supported by grants from the "Excellence Initiative – Research University" program for the years 2020–2026 for the University of Wrocław BPIDUB.4610.651.2021. I acknowledge the contribution of Professor W. Gac to the TPD experiment. The research was carried out with the equipment purchased thanks to the financial support of the European Regional Development Fund in the framework of the Polish Innovation Economy Operational Program (contract no. POIG.02.01.00-06024/09–Centre of Functional Nanomaterials).

Notes and references

1 O. M. Yaghi, M. O'Keeffe, N. W. Ockwig, H. K. Chae, M. Eddaoudi and J. Kim, *Nature*, 2003, **423**, 705–714.
2 J. Liu, P. K. Thallapally, B. P. McGrail, D. R. Brown and J. Liu, *Chem. Soc. Rev.*, 2012, 2308–2322.
3 L. Jiao, J. Y. R. Seow, W. S. Skinner, Z. U. Wang and H.-L. Jiang, *Mater. Today*, 2019, **27**, 43–68.
4 W. Tu, Y. Xu, S. Yin and R. Xu, *Adv. Mater.*, 2018, **30**, 1707582.
5 J. Gascon, A. Corma, F. Kapteijn and F. X. L. I. Xamena, *ACS Catal.*, 2014, **4**, 361–378.
6 A. Bavykina, N. KolobovIl, S. Khan, J. A. Bau, A. Ramirez and J. Gascon, *Chem. Rev.*, 2020, **120**, 8468–8535.
7 J. Lin, J. Ouyang, T. Liu, F. Li, H. Ho-Yung Sung, I. Williams and Y. Quan, *Nat. Commun*, 2023, **14**, 7757.
8 F. Gao, R. Yan, Y. Shu, Q. Cao and L. Zhang, *RSC Adv.*, 2022, **12**, 10114–10125.
9 C. Wang, J. Kim, J. Tang, M. Kim, H. Lim, V. Malgras, J. You, Q. Xu, J. Li and Y. Yamauchi, *Chem*, 2020, **6**, 19–40.
10 D. Liu, W. Gu, L. Zhou, L. Wang, J. Zhang, Y. Liu and J. Lei, *Chem. Eng. J.*, 2022, **427**, 131503.
11 J. Fang, Z. Huang, S. Zhao, Z. Chen, W. Huang, Z. Liang and Y. Qiu, *Colloids Surf., A*, 2024, **703**, 135279.
12 B. Feng, Q. Xu, X. Wu, Ch. Ye, Y. Fu, D.-L. Chen, F. Zhang and W. Zhu, *Appl. Surf. Sci.*, 2021, **557**, 149837.
13 Y. Shao, J. Zhang, H. Jiang and R. Chen, *Ind. Eng. Chem. Res.*, 2021, **60**, 5806–5815.
14 S. Ding, C. Zhang, Y. Liu, H. Jiang and R. Chen, *Appl. Surf. Sci.*, 2017, **425**, 484–491.
15 Q. Zhu, X. Lu, S. Ji, H. Li, J. Wang and Z. Li, *J. Catal.*, 2022, **405**, 499–507.
16 A. W. Augustyniak and A. M. Trzeciak, *ChemCatChem*, 2021, **13**, 2145.
17 A. Staubitz, A. P. M. Robertson and I. Manners, *Chem. Rev.*, 2010, **110**, 4079–4124.
18 W. Chen, X. Duan, G. Qian, D. Chen and X. Zhou, *ChemSusChem*, 2015, **8**, 2927–2931.
19 S. Akbayrak, Y. Tonbul and S. Özkar, *Appl. Catal., B*, 2016, **198**, 162–170.
20 M. Shingole, S. Banerjee, P. Ruz, A. Kumar, P. Sharmac and V. Sudarsan, *Catal. Sci. Technol.*, 2024, **14**, 63–6350.
21 X. Qiu, J. Liu, S. Qiu, P. Huang, H. Chu, Y. Zou, H. Zhang, F. Xu and L. Sun, *Sustainable Energy Fuels*, 2021, **5**, 2301–2312.
22 L. Wang, H. Li, W. Zhang, X. Zhao, J. Qiu, A. Li, X. Zheng, Z. Hu, R. Si and J. Zeng, *Angew. Chem., Int. Ed.*, 2017, **56**, 4712–4718.
23 C. Wang, J. Tuninetti, Z. Wang, C. Zhang, R. Ciganda, L. Salmon, S. Moya, J. Ruiz and D. Astruc, *J. Am. Chem. Soc.*, 2017, **139**, 11610–11615.
24 K. S. Eom, K. W. Cho and H. S. Kwon, *Int. J. Hydrogen Energy*, 2010, **35**, 181–186.
25 S. K. Oh, D. H. Song, H. W. Kim, D. R. Sohn, K. S. Hong, M. H. Lee, S. H. Son, E. A. Cho and H. S. Kwon, *J. Alloys Compd.*, 2019, **806**, 643–649.
26 Q. Zhao, B. Espuche, N. Kang, S. Moya and D. Astruc, *Inorg. Chem. Front.*, 2022, **9**, 4651–4660.
27 X. Zhao, Y. Chang, W.-J. Chen, Q. Wu, X. Pan, K. Chen and B. Weng, *ACS Omega*, 2022, **7**, 17–31.
28 R. S. Oosthuizen and V. O. Nyamori, *Platinum Met. Rev.*, 2011, **55**, 154–169.
29 H. Liu, M. Huang, W. Tao, L. Han, J. Zhang and Q. A. Zhao, *Nanomaterials*, 2024, **14**, 549.
30 Q. Xie, X. Liu, Y. Xing, L. Huang, W. Lei, S. Zhang and H. Zhang, *Phys. Chem. Chem. Phys.*, 2025, **27**, 3401–3411.
31 J. A. R. Navarro, E. Barea, J. M. Salas, N. Masciocchi, S. Galli, A. Sironi, C. O. Ania and J. B. Parra, *Inorg. Chem.*, 2006, **45**, 2397–2399.
32 Y. Wang, Z. Zhum, K. Xu, W. Guo, T. Yu, M. He, W. Wei and T. Yang, *ACS Appl. Nano Mater.*, 2021, **4**, 2118–2125.
33 D. Giasafaki, G. Charalambopoulou, C. Tampaxis, K. Dimos, D. Gournis, A. Stubos and T. Steriotis, *Carbon*, 2016, **98**, 1–14.
34 A. Lazzarini, R. Pellegrini, A. Piovano, S. Rudić, C. Castan-Guerrero, P. Torelli, M. R. Chierotti, R. Gobetto, C. Lamberti and E. Groppo, *Catal. Sci. Technol.*, 2017, **7**, 4162–4172.
35 J. Wu, L. Wang, B. Lv and J. Chen, *ACS Appl. Mater. Interfaces*, 2017, **9**, 14319–14327.
36 W. Chen, J. T. Li, C. Ge, Z. Yuan, W. A. Algozeeb, P. A. Advincula, G. Gao, J. Chen, K. Ling, C. H. Choi, E. A. McHugh, K. M. Wyss, D. X. Luong, Z. Wang, Y. Han and J. M. Tour, *Adv. Mater.*, 2022, **34**, 2202666.
37 M. Li, L. Qiu, I. Popovs, W. Yang, A. S. Ivanov, T. Kobayashi, B. P. Thapaliya, D. Moitra, X. Yu, Z. Wu, Z. Yang and S. Dai, *Angew. Chem.*, 2023, **62**, e202302684.
38 R. V. Chaudhari, R. Jaganathan, D. S. Kolhe, G. Emig and H. Hofmann, *Chem. Eng. Sci.*, 1986, **41**, 3073–3081.

39 L. Li, W. Yang, Q. Yang, Q. Guan, J. Lu, S.-H. Yu and H.-L. Jiang, *ACS Catal.*, 2020, **10**, 7753–7762.
40 K. Jiang, J. Chang, H. Wang, S. Brimaud, W. Xing, R. J. Behm and W.-B. Cai, *ACS Appl. Mater. Interfaces*, 2016, **8**, 7133–7138.
41 Z. Zhang, J. Lu, B. Zhang, W. Shi, Y. Guo and F. Cui, *Environ. Sci.: Nano*, 2020, **7**, 2117–2129.
42 X. Wang, C. Han, H. Li, P. Su, N. Ta, Y. Ma, Z. Huang and J. Liu, *Nano Res.*, 2023, **16**, 290–298.
43 S. Chen, P. Li, S. Xu, X. Pan, Q. Fu and X. Bao, *J. Mater. Chem. A*, 2018, **6**, 1832–1839.
44 Z. Duan, X. Wang, R. Wei, Q. Lei and H. Chen, *Appl. Surf. Sci.*, 2023, **613**, 156166.
45 X. Deng, J. Wang, N. Guan and L. Li, *Cell Rep. Phys. Sci.*, 2022, **9**, 101017.
46 S. V. Sawant, M. D. Yadav, S. Banerjee, A. W. Patwardan, J. B. Joshi and K. Dasgupta, *Int. J. Hydrogen Energy*, 2021, **46**, 39297–39314.